ELSEVIER

Journal of Alloys and Compounds 317–318 (2001) 603–606

Journal of ALLOYS AND COMPOUNDS

www.elsevier.com/locate/jallcom

Electrochemical behavior of Au–Gd alloys

F. Rosalbino[a,*], E. Angelini[a], S. Spriano[a], C. Antonione[a], S. Delfino[b], D. Macciò[b], A. Saccone[b]

[a]*Dipartimento di Scienza dei Materiali e Ingegneria Chimica, Politecnico di Torino, C.so Duca degli Abruzzi 24, I-10129 Torino, Italy*
[b]*Dipartimento di Chimica e Chimica Industriale, Università di Genova, Via Dodecaneso 31, I-16146 Genoa, Italy*

Abstract

The electrochemical behavior of five Au–Gd alloys in three alkaline electrolytes has been characterised by the cyclic voltammetry technique. The alloys studied were: $Au_{96}Gd_4$, $Au_{69.5}Gd_{30.5}$, $Au_{53}Gd_{47}$, $Au_{25}Gd_{75}$ and Au_5Gd_{95}. The electrolytes used were: (i) Na_2CO_3, (ii) $Na_2B_4O_7$ and (iii) NaF — each with a concentration of 0.2 M. It was observed that the alloy composition, rather than the microstructure, plays an important role in determining the electrochemical behavior of these alloys. The oxidation process is more influenced by the specific adsorption of $B_4O_7^{2-}$ and F^- than by the CO_3^{2-}.

Keywords: Au–Gd alloys; Intermetallic phases; Electrochemical behavior; Cyclic voltammetry; Anion adsorption

1. Introduction

Au–Gd alloys have been extensively studied from the standpoint of microstructural and morphological features [1–8]. However little or no information exists about their electrochemical behavior. The present study is an attempt to obtain this information on selected Au–Gd alloys in three alkaline electrolytes. In fact, gold alloys are widely used in the electronics industry where they are exposed to a range of uncontrolled environments that may be much more aggressive than air-conditioned computer rooms [9].

2. Experimental details

2.1. Alloy sample preparation

Alloys of the following composition were investigated: $Au_{96}Gd_4$ (96.78 mass% Au), $Au_{69.5}Gd_{30.5}$ (74.05 mass% Au), $Au_{53}Gd_{47}$ (58.55 mass% Au), $Au_{25}Gd_{75}$ (29.45 mass% Au) and Au_5Gd_{95} (6.18 mass% Au). They were prepared using pure Gd (99.9 mass% purity, Newmet Koch, Hertford, UK) and Au (99.99 mass% purity, Johnson Matthey, London, UK). The two metals in required amounts (0.8–1 g each sample) were enclosed in sealed molybdenum crucibles, under argon atmosphere, and then melted in an induction-heated furnace according to the procedure described before [8]. Repeated shaking of the crucibles during the melting was carried out to ensure homogenisation. No post-solidification heat treatments were made.

2.2. Microstructural characterisation

Prior to electrochemical evaluation, all alloys were characterised by various techniques such as DTA, XRD, light microscopy, SEM and EDS to verify that respective microstructures are in agreement with that predicted from the Au–Gd phase diagram [8].

For the sake of clarity, the details of the procedure are not included here but are available from the authors. Table 1 summarises the observations from microstructural evaluation.

2.3. Electrochemical evaluation

The electrochemical behavior of the alloys was evaluated by the cyclic voltammetry technique starting from the open circuit potential of respective alloys. The counter-electrode was a 10-cm^2 platinum grid and a saturated calomel electrode (SCE) was used as reference. The scan rate dE/dt was 50 mV/s. After five to six cycles, the potential-current density profiles, $E–j$ curves, reached a quasi-steady state and the data reported represent the fifth or sixth cycle scan. As Gd is highly unstable in electrolytes of low pH ($\leq$7), the electrochemical behavior of the alloys was evaluated in alkaline electrolytes. The electrolytes chosen were: (i) 0.2 M Na_2CO_3, (ii) 0.2 M $Na_2B_4O_7$ and (iii) 0.2 M NaF at 25$\pm$1°C. The pH's of the three electrolytes were 8.3, 9.1, 11.8, respectively. For com-

*Corresponding author.

0925-8388/01/$ – see front matter
PII: S0925-8388(00)01395-5

Table 1
Au–Gd alloys: micrographic and X-ray diffraction data of the selected samples used for electrochemical characterisation

Composition, at% Au	Composition, wt% Au	Micrographic appearance (and microprobe analysis)	EPMA results		Diffraction lines observed in the powder photographs	Structure type/ Pearson symbol	Lattice parameters obtained (pm)	Lattice parameters (pm) of the pure phases as reported in the literature
			At% Au	At% Gd				
5	6.18	Gd_2Au+ eutectic ((Gd)+Gd_2Au)	33.2	66.9	(αGd)	Hexagonal hP2-Mg	a=363.2 c=578.0	αGd a=363.36 [10] c=578.10
					$AuGd_2$	Orthorhombic oP12-Co_2Si	a=711.9 b=497.8 c=898.1	$AuGd_2$ a=711.4(4) [8] b=495.8(3) c=899.5(6)
25	12.22	Gd_2Au+ eutectic ((Gd)+Gd_2Au)	33.1	66.9	(αGd)	Hexagonal hP2-Mg	a=363.2 c=578.4	–
					$AuGd_2$	Orthorhombic oP12-Co_2Si	a=711.5 b=496.8 c=899.3	–
53	58.55	GdAu + Gd_3Au_4	50.6	49.4	AuGd	Cubic cP2-CsCl	a=358.8	AuGd a=358.8(3) [8]
			52.8	47.2	Au_4Gd_3	Trigonal hR42-Pd_3Pu_4	a=1350.3 c=599.1	Au_4Gd_3 a=1349.8(6) [8] c=599.5(3)
69.5	74.05	$GdAu_2$+ eutectic ($GdAu_2$+ $GdAu_3$)	66.8	33.2	Au_2Gd	Tetragonal tI6-$MoSi_2$	a=372.3 c=903.0	Au_2Gd a=372.2(2) [8] c=900.2(6)
96	96.78	(Au)+ eutectic ((Au)+$GdAu_6$)	99.3	0.7	(Au)	Cubic cF4-Cu	a=408.4	Au a=407.82 [11]

parison purposes, the electrochemical tests were also performed on pure gold.

3. Results and discussion

Fig. 1 shows the cyclic voltammograms, E–j curves, for the Gd-rich alloys in 0.2 M Na_2CO_3 solution. On the anodic side, a sharp oxidation peak, at +0.38 V, is observed. It corresponds to the formation of gadolinium hydroxide [12], according to the reaction:

$$Gd + 3H_2O \rightarrow Gd(OH)_3 + 3H^+ + 3e^- \quad (1)$$

The sudden increase of the anodic current density at potentials >1 V can be attributed to the onset of oxygen evolution reaction:

$$2H_2O \rightarrow O_2 + 4H^+ + 4e^- \quad (2)$$

On the cathodic side, the sharp peak located at ≈0.0 V is attributed to the reduction of $Gd(OH)_3$ a reversal of reaction (1) above.

The cyclic voltammograms for the Au-rich alloys and pure gold in 0.2 M Na_2CO_3 solution are shown in Fig. 2. The behavior of the alloys is similar to that of pure gold: however, small differences exist in the j vs. E profiles. The broad peak located at ≈ +0.55 V corresponds to the onset of gold oxide formation [13]:

$$2Au + 3H_2O \rightarrow Au_2O_3 + 6H^+ + 6e^- \quad (3)$$

while the sharp peak located at ≈ +0.15 V on the cathodic side is attributed to the corresponding reverse reaction.

As in the case of Gd-rich alloys, the abrupt increase in

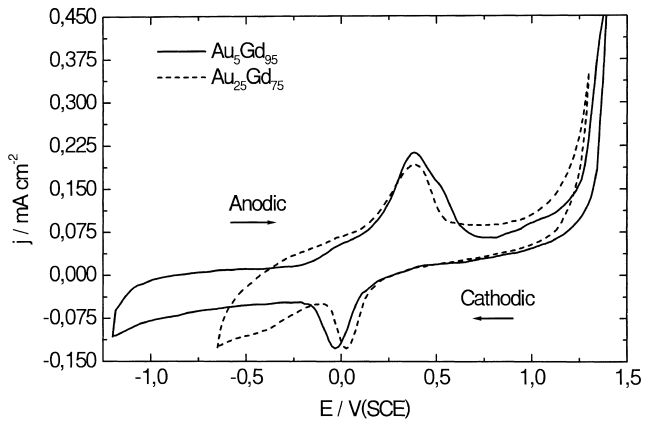

Fig. 1. Cyclic voltammograms for Gd-rich alloys in 0.2 M Na_2CO_3 solution.

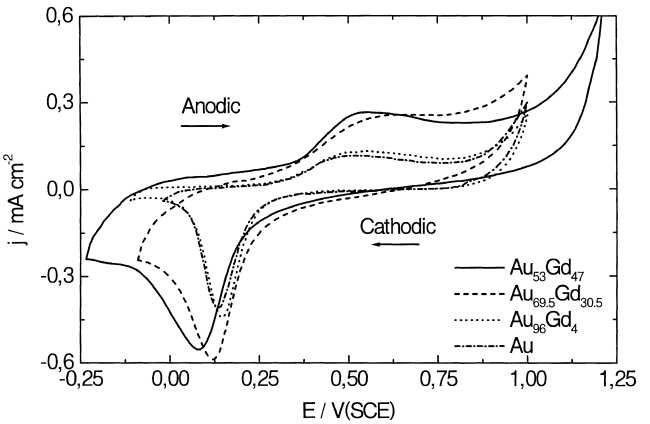

Fig. 2. Cyclic voltammograms for Au-rich alloys in 0.2 M Na_2CO_3 solution.

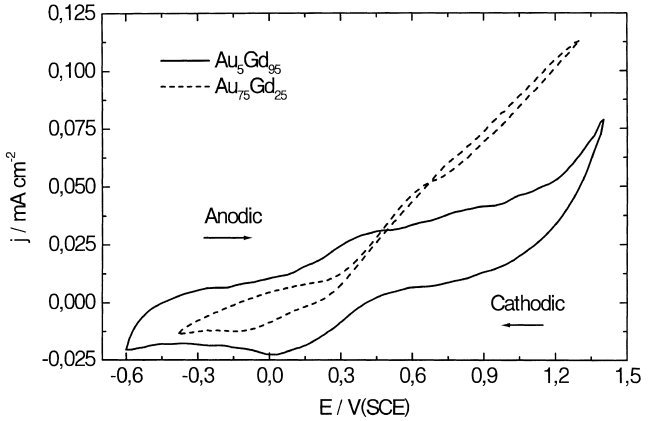

Fig. 3. Cyclic voltammograms for Gd-rich alloys in 0.2 M $Na_2B_4O_7$ solution.

current density observed at high anodic potentials corresponds to the onset of oxygen evolution reaction.

On the basis of the above data we infer that the oxidation behavior of Au–Gd alloys is not significantly influenced by the adsorption of CO_3^{2-} ions.

Fig. 3 reports the cyclic voltammograms for Gd-rich alloys in 0.2 M $Na_2B_4O_7$ solution. A comparison with Fig. 1 indicates that the anodic and cathodic current peaks observed in Na_2CO_3 are greatly suppressed. This behavior is explained by the formation of a strongly adsorbed layer of $B_4O_7^{2-}$ ions in accordance to the following reaction [14]:

$$Gd + B_4O_7^{2-} \rightarrow Gd - (B_4O_7)_{ads} + 2e^- \quad (4)$$

It appears that the chemisorbed layer of anions forming a coordinate type of bond exerts a steric effect and thus prevents reaction (1) from occurring on the electrode surface.

The cyclic voltammograms of Au and Au-rich alloys in $Na_2B_4O_7$ solution are shown in Fig. 4. The *j* vs. *E* profiles are very similar to Fig. 1, but the anodic oxidation peak is

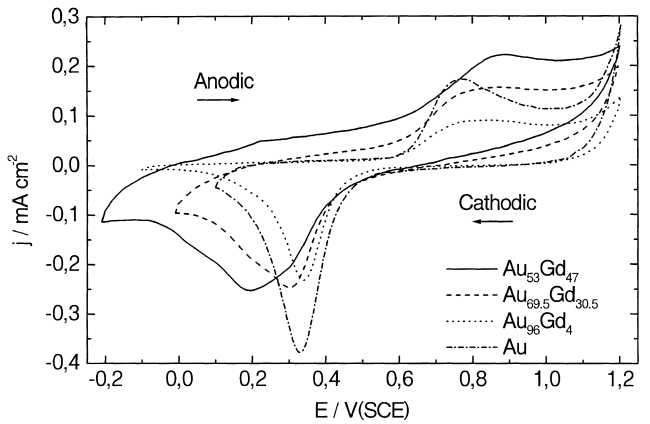

Fig. 4. Cyclic voltammograms for Au-rich alloys in 0.2 M $Na_2B_4O_7$ solution.

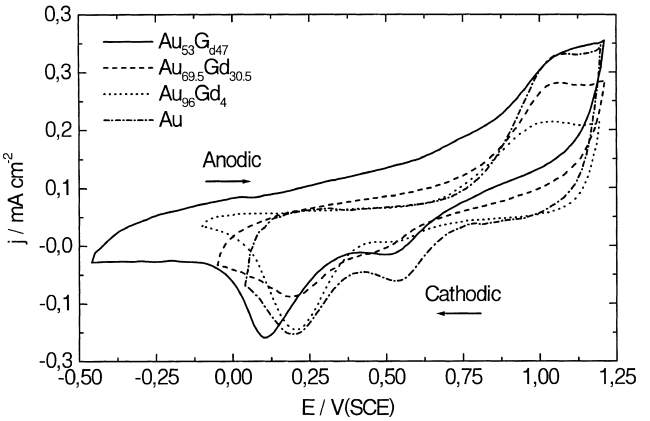

Fig. 5. Cyclic voltammograms for Au-rich alloys in 0.2 M NaF solution.

shifted towards more positive potentials and is located at $\approx +0.88$ V. This is explained by the formation of an adsorbed layer of $B_4O_7^{2-}$ ions at the electrode surface. This layer exerts a blocking effect of active surface states. Consequently gold oxide formation may take place only if accompanied by desorption of the anions:

$$Au - (B_4O_7^{2-})_{ads} - Au + 3H_2O \rightarrow Au_2O_3 + 6H^+ + 6e^- + B_4O_7^{2-} \quad (5)$$

occurring at sufficiently high potentials [14].

The shift of the onset potential for the anodic oxidation process is more accentuated in 0.2 M NaF solution, as shown in the cyclic voltammograms for Au and Au-rich alloys (Fig. 5). Here again the *j*–*E* profiles are very similar and characterised by a sharp anodic peak, at $\approx +1.05$ V, close to the onset of oxygen evolution reaction. This marked shift of the anodic oxidation potential may be attributed to the higher strength of F^- ions adsorption with respect to those of $B_4O_7^{2-}$ or to a possible 'reactive coverage' of the electrode surface [15] where the adsorption of F^- ions is followed by an electrochemical reaction. The onset of anodic dissolution of gold followed by the cathodic deposition of the metal may take place [16]. At present differential capacity measurements are in progress in order to confirm this hypothesis.

The electrochemical behavior of the Gd-rich alloys is presented in Fig. 6. The presence of a sharp peak located at $\approx +0.6$ V, on the anodic side of voltammograms is observed. This peak is attributed to an anodic dissolution reaction between gadolinium and fluoride ions:

$$Gd + 4F^- \rightarrow GdF_4^- + 3e^- \quad (6)$$

4. Conclusions

Because of the large difference in the standard electrode potential values of the two constituent elements (Au, $E^0 = +1.50$ V (NHE) and Gd, $E^0 = -2.40$ V (NHE)), the electrochemical behavior of the Au–Gd alloys appears to

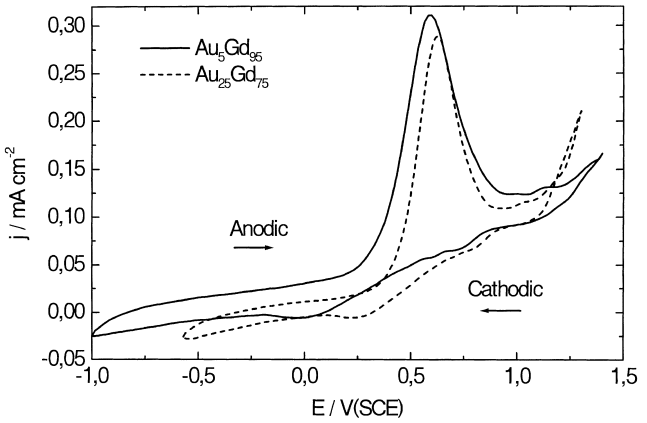

Fig. 6. Cyclic voltammograms for Gd-rich alloys in 0.2 M NaF solution.

be strongly influenced by their chemical composition. The significant difference in the microstructure of various alloys was not reflected in their electrochemical behavior.

In solutions containing weakly adsorbed anions, as CO_3^{2-}, the gold content of the alloys seems to be the predominant factor affecting the onset potential for the anodic oxidation process. The presence of specifically adsorbed anions, such as $B_4O_7^{2-}$ and F^-, noticeably modifies the oxidation behavior because of their strong interactions with the electrode surface. In fact, $B_4O_7^{2-}$ ions exert a blocking effect on the metal surface. The effect is particularly strong with Gd-rich alloys. Fluoride ions seem to be involved in a possible anodic dissolution reaction. Differential capacity measurements are in progress in order to confirm this hypothesis.

Acknowledgements

The planning and development of the investigation here presented form a part of an Italian National Research Project entitled: 'Leghe e composti intermetallici. Stabilità termodinamica, proprietà fisiche e reattività'. The authors would like to thank the Italian Ministero della Ricerca Scientifica e Tecnologica (Programmi di Ricerca Scientifica di Rilevante Interesse Nazionale) for the financial support afforded them. Partial financial support was obtained also in the framework of the Italian 'Progetto finalizzato Materiali Speciali per Tecnologie Avanzate II'.

References

[1] O.D. Mc Master, K.A. Gschneidner Jr., G. Bruzzone, A. Palenzona, J. Less-Common Met. 25 (1971) 135.
[2] O.D. McMaster, K.A. Gschneidner Jr., J. Less-Common Met. 30 (1971) 325.
[3] C.C. Chao, H.L. Luo, P. Duwez, J. Appl. Phys. 34 (1963) 1971.
[4] K.A. Gschneidner Jr., Acta Crystallogr. 18 (1965) 1082.
[5] N.C. Baenziger, J.L. Moriarty, Acta Crystallogr. 14 (1961) 948.
[6] A.E. Dwight, J.W. Downej, R.A. Conner, Acta Crystallogr. 22 (1967) 745.
[7] V. Sadagopan, B.C. Giiessen, N.J. Grant, J. Less-Common Met. 14 (1968) 279.
[8] A. Saccone, M.L. Fornasini, D. Macciò, S. Delfino, Intermetallics 4 (1996) 111.
[9] R.P. Frankenthal, Sol. State Electron. 33 (1990) 69.
[10] K.A. Gschneidner Jr., F.W. Calderwood, Intra rare earth binary alloys: phase relationships, lattice parameters and systematics', in: K.A. Gschneidsner Jr., J. Eyring (Eds.), Handbook on the Physics and Chemistry of Rare Earths, Vol. 8, North Holland, Amsterdam, 1986, p. 4.
[11] P. Villars, A. Prince, H. Okamoto, Handbook of Ternary Alloy Phase Diagrams, Vol. 1, ASM International, Materials Park, Ohio, USA, 1985.
[12] M. Pourbaix, Atlas of Electrochemical Equilibria in Aqueous Solution, Pergamon and CEBELCOR, Oxford, 1966.
[13] J.P. Hoare, The Electrochemistry of Oxygen, Interscience, New York, 1968.
[14] B.E. Conway, H. Angerstein-Kozlowska, F.C. Ho, J. Klinger, B. MacDougall, S. Gottsfeld, Faraday Discuss. Chem. Soc. Lond. 56 (1973) 199.
[15] K.J. Vetter, J.W. Schulze, Ber. Bunsenges. Phys. Chem. 76 (1972) 920.
[16] G. Just, R. Landsberg, Z. Phys. Chem. 226 (1964) 183.